Application of Extended X-ray Absorption Fine Structure Technique to Ni in the High-T, Superconductor $YBa_2Cu_{3-x}Ni_xO_{7-y}$

C. H. Chou (周鑑恒) and S. F. Tsai (蔡尚芳)

Department of Physics, National Taiwan University

Taipei, Taiwan IO 764, R. 0. C.

(Received June 15, 1990; revised manuscript received July 20, 1990)

We present a study of crystalline $Ni(OH)_2$ and the high-T_c superconductor $YBa_2Cu_{3-x}Ni_xO_{7-y}$ ($x \approx$ *0.12)* by extended x-ray-absorption fine structure (EXAFS). By the use of the theoretical back-scattering amplitudes and phase-shift functions, the EXAFS spectra ($k^n\chi(k)$) of $NiO, Ni(OH)_2$ and $YBa_2Cu_{3-x}Ni_xO_{7-y}$ have been simulated in order to aid us to reconfirm the analysis results. The Ni-0 bond distance in crystalline $Ni(OH)_2$ has been determined as (2.05 ~ 2.06) Å. This is accomplished either by using the experimental data of NiO or by using the theoretical back-scattering amplitudes and phase-shift functions. Both were used in this study. Various methods of analysis yield consistent values of (1) the distances between the oxygen atoms and the nickel atom and (2) the number of oxygen atoms around a nickel atom in $YBa_2Cu_{3-x}Ni_xO_{7-y}$. Our results indicate that the incorporated Ni atoms replace Cu atoms at the Cu(1) site in $YBa_2Cu_3O_{7-y}$. This work demonstrates that EXAFS can be used to provide information about the position of the incorporated atoms in $YBa_2Cu_{3-x}Ni_xO_{7-y}$.

I. INTRODUCTION

The discovery of high-temperature superconductivity in several oxides, such as $YBa_2Cu_3O_{7-y}$, has raised many different speculations about possible new electron-pairing mechanisms. The structural and superconducting properties of the material $YBa_2Cu_3O_{7-y}$ have been investigated.[1,2,3,4] The systematic substitution of impurity atoms (in this paper: nickel atoms for copper atoms) and the determination of preferential substitutent effects on superconducting properties provide ways to probe superconductivity in $YBa_2Cu_3O_{7-y}$.[5,6]

However, x-ray diffraction data have not revealed how the incorporated nickel ions, which partially substitute for the copper, are distributed over the two copper sites (i.e., the chain site and the Cu-0 plane, labeled Cu(1) and Cu(2)) present in the structure of $YBa_2Cu_3O_{7-y}$.

Extended x-ray-absorption fine structure (EXAFS)[7] has been shown to be a useful tool to determine the local structure surrounding an x-ray-absorbing atom. Many structural parameters such as interatomic distances and the number of coordinating atoms can be

determined from experimental EXAFS spectra.

Because there are two nonequivalent Cu sites which are associated with five different Cu-0 bond distances and which may be occupied by the incorporated Ni atoms, the application of the EXAFS technique to Ni in $YBa_2Cu_{3-x}Ni_xO_{7-y}$ becomes an elaborate process. Nevertheless, by considering the character of the EXAFS spectra (K-edge absorption of Ni in the materials) and employing versatile methods of analysis, we have been able to draw firm conclusions about the local structure of Ni in $YBa_2Cu_{3-x}Ni_xO_{7-y}$ and then to verify successfully the sites of the Ni atoms.

II. SAMPLE PREPARATION AND MEASUREMENT

The samples were prepared by mixing appropriate amounts of $Y_2O_3, BaCO_3, CuO$ and NiO powders of at least 99.9%. The mixtures were calcined in air at 950° C for 24 hours with several intermediate grindings. The resultant powders were ground and pressed into pellets. These pellets were then sintered in a continuous flow of oxygen at 950° C for another 24 hours. Finally an annealing process at 950°C in an O_2 environment for 6 hours and cooling in the furnace preceded the various measurements.

The EXAFS measurements were performed on the beam line at the National Synchrotron Light Source (NSLS). The absorption spectra of NiO and $Ni(OH)_2$ were measured by means of the transmission experiments; the absorption spectrum of $YBa_2Cu_{3-x}Ni_xO_{7-y}$ was obtained by means of the excitation method (i.e. fluorescent experiments).

III. DATA AND ANALYSIS

The linear K-shell absorption coefficients (denoted by μ) of Ni in $NiO, Ni(OH)_2$ and $YBa_2Cu_{3-x}Ni_xO_{7-y}$ are shown in Fig. 1 (a), (b), (c) respectively.
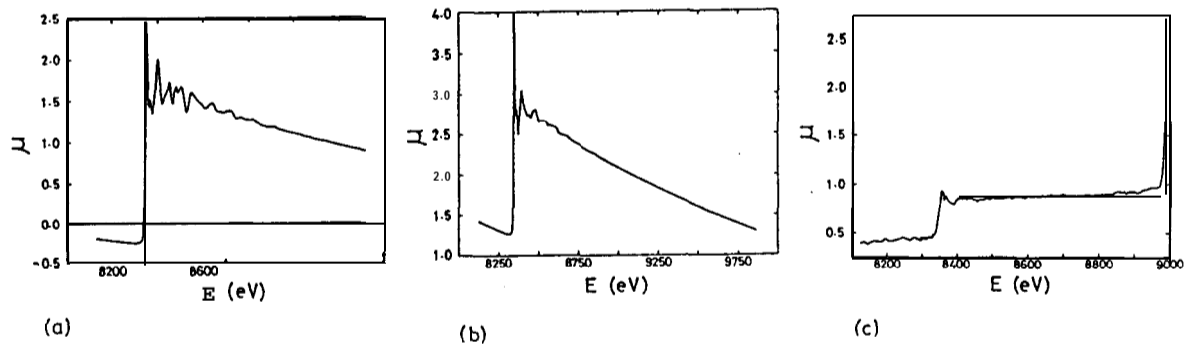

FIG. 1.   The linear absorption coefficient μ obtained from transmission of (a) NiO, (b) $Ni(OH)_2$, and the linear absorption coefficient μ obtained from fluorescence of (c) $YBa_2Cu_{3-x}Ni_xO_{7-y}$.

(1) Utilizing the one-electron, single-scattering approximation, (2) taking the average of the polarization effect, (3) taking the contribution of the thermal fluctuation and static disorder and (4) taking many-body effects into account, we express the oscillatory modulation of the linear K-shell absorption coefficient as

$$\chi(k) = \frac{\mu(E) - \mu_0(E)}{\mu_0(E)}$$

$$= \sum_j \frac{N_j}{k R_j^2} S_0^2(k) F_j(k) \exp(-2\sigma_j^2 k^2) \exp(\frac{-2(R_j - \Delta)}{\lambda_j(k)}) \sin(2kR_j + \phi_j(k)) \qquad (1)$$

in which μ_0 is the structureless absorption coefficient of the isolated atom in question, k is the wave vector of the ejected photoelectron, N_j is the number of equivalent scatterers of type j at distance R_j, and $F_j(k)$ is the magnitude of the back-scattering amplitude from each of the N_j neighboring atoms of type j with a Debye-Waller factor $\exp(-2\sigma_j^2 k^2)$ to account for thermal vibration and static disorder; $\sin(2kR_j + \phi_j(k))$ is the sinusoidal interference term, with $\phi_j(k)$ being the composite phase-shift function which contains contributions from both the absorber and the scatterer. S_0 is the amplitude-reduction factor representing shake-up and shake-off effects of the central atom. The term $\exp(-2(R_j - \Delta)/\lambda_j(k))$ is due to inelastic scattering and decay of the core hole, with λ_j being the mean free path and A being a " Core radius" . The latter two terms reflect many-body effects.

The x-ray energy E is converted into the wave vector k by means of the equation:

$$k = [2m_e(E - E_0)/\hbar^2]^{1/2} \qquad (2)$$

Here, E_0 in general, being in the vicinity' of the edge, is the so-called threshold energy, m_e is the mass of the electron, and energy and wave vector are conventionally expressed in the units eV and Å^{-1} respectively.

Recent studies[9,10] have indicated that the single scattering approximation is adequate to much smaller energies than previously believed, provided that calculations at these smaller energies are done with the curved-wave formalism, such that the curvature of the outgoing and scattered photoelectron wave functions is taken into account. That is, the EXAFS expression, according to Eq. (I), is valid well into the XANES region" (to ~15eV above the edge, ca. 2Å^{-1}). Therefore we calculated the Fourier transform over the range that begins at $\sim 2\text{Å}^{-1}$.

Depending on the facilities that are available for experiments, supplementary techniques may also be employed during the analysis process. In this work, tasks have been accomplished by means of the processes introduced below: 1) extraction of $\chi(k)$ data, 2) Fourier filtering, 3) analysis of the Fourier-filtered data.

The structures of crystalline NiO and $Ni(OH)_2$ are well known, however, the Ni-0 bond distance of crystalline $Ni(OH)_2$ is uncertain (see Table I). Therefore, one can use crystalline NiO as a model sample to determine the Ni-0 bond distance of the unknown sample $Ni(OH)_2$. We extracted the $\chi(k)$ data of each of NiO and $Ni(OH)_2$ by choosing E_0

TABLE I. Lattice distances and coordination of the first two shells around Ni in NiO and $Ni(OH)_2$

Crystalline NiO Coordination			Crystalline $Ni(OH)_2$ Coordination		
Shell	Occupancy	Distance, Å	Shell	Occupancy	Distances, A
1	6	0	2.084	1	3	0	-2.
2	12	Ni	2.947	2	3	Ni	-3.

at the first peak of the absorption coefficient $\mu(E)$, and by performing the background sub-traction and normalization. We obtained magnitudes of the Fourier transform of the $\chi(k)$ data sets of NiO and $Ni(OH)_2$, shown in Fig. 2(a)(b), by multiplying the $\chi(k)$ data by k^2 and k^3, and by transforming over the k ranges $2.28 - 12.28$ Å^{-1} and $2.33 - 13.08$ Å^{-1} respectively.   We used the standard process of determining the bond distance of the unknown sample to obtain the total phases of the Fourier-filtered $\chi(k)$ spectra (containing the contribution of the first shell corresponding to the first peak in Fig. 2(a) (b)) of NiO and
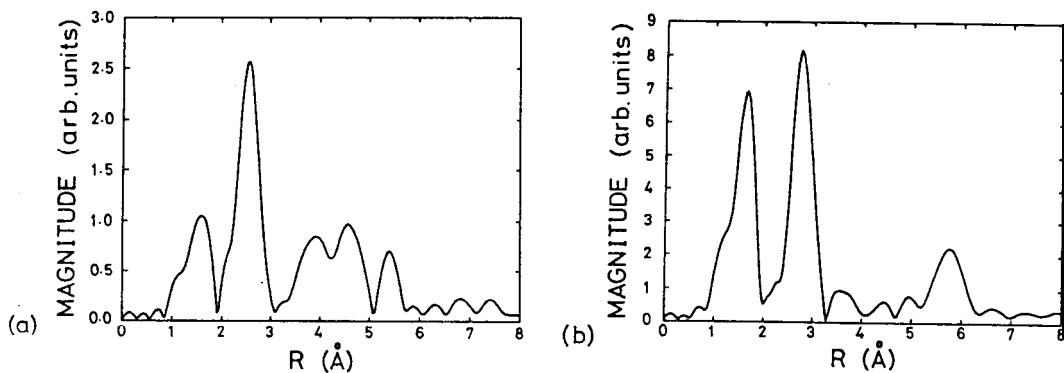

FIG. 2.   The magnitude of the Fourier transform of (a) the $k^2\chi(k)$ spectrum of crystalline NiO, and (b) the $k^3\chi(k)$ spectrum of crystalline $Ni(OH)_2$

$Ni(OH)_2$. Fitting by a straight line the difference in these total phase functions (Ni-0 pair) of NiO and $Ni(OH)_2$ (shown in Fig. 3(a)) yielded the unknown Ni-0 bond distance of $Ni(OH)_2$ as (2.063 ± 0.003) Å. Repeating the same process except to choose E_0 at the half-height point of the absorption edge, we determined the unknown Ni-0 bond distance of $Ni(OH)_2$ as (2.055 ± 0.003) Å (shown in Fig. 3(b)).

After determining the Ni-0 bond distance in crystalline $Ni(OH)_2$ and neglecting many-body effects, we simulated the $k^3\chi(k)$ function of $Ni(OH)_2$ (shown in Fig. 4(a)), which contains the first two shells ($R_1 = 2.051$ Å; $R_2 = 3.184$ Å; $N_1 = 3$; $N_2 = 3$; $\sigma_1^2 = 0.002$; $\sigma_2^2 = 0.002$), based on the theoretical phase-shift functions and back-scattering amplitudes calculated by Teo and Lee,[12] and we used the simulated '$Ni(OH)_2$' as the model sample to reconfirm the Ni-0 bond distance of crystalline $Ni(OH)_2$. We obtained the magnitude of the Fourier transform of the simulated $k^3\chi(k)$ data by transforming over the k range from 2.15 to 13.25 Å^{-1} (shown in Fig. 4(b)).
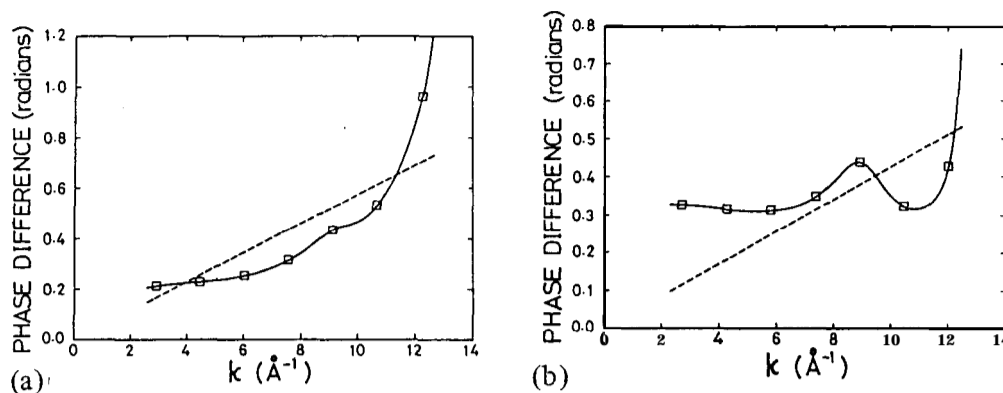
FIG. 3. The plot of the difference in the total phase functions of the Fourier-filtered spectra (first shell) of the unknown, $Ni(OH)_2$, and the model, NiO, as a function of k with the value of E_0 chosen at (a) the first peak of the absorption coefficient μ and (b) the half-height point of the absorption edge. The straight dashed line was obtained by fitting to the difference of the total phases of the Ni-0 pairs in NiO and $Ni(OH)_2$.
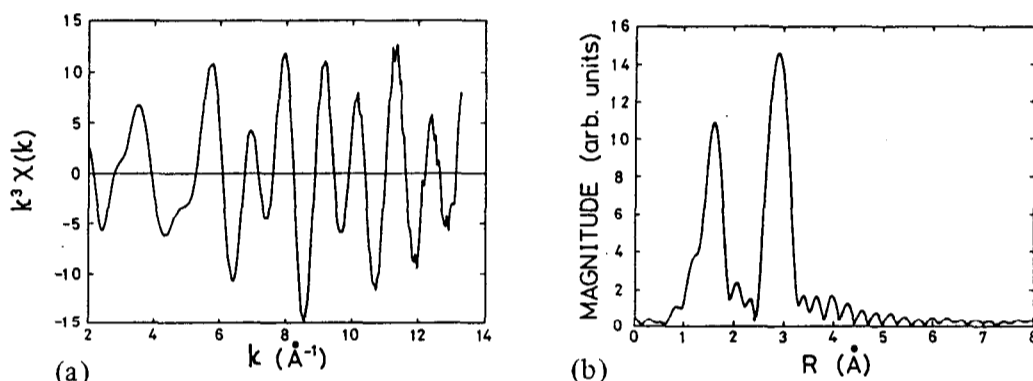

FIG. 4. (a) The simulated $k^3\chi(k)$ data of the first two shells of $Ni(OH)_2$. (b) The magnitude of the Fourier transform of the simulated $k^3\chi(k)$ spectrum.

In Fig. 5(a), curve A refers to the Fourier-filtered $k^3\chi(k)$ spectrum (first shell) of the simulated data; curve B refers to the Fourier-filtered $k^3\chi(k)$ spectrum (first shell) of the EXAFS function of $Ni(OH)_2$ extracted on the basis of E_0 being the first peak of the μ spectrum; curve C refers to the Fourier-filtered $k^3\chi(k)$ spectrum (first shell) of the EXAFS functions of $Ni(OH)_2$ extracted on the basis of E_0 being 8 eV above the first peak of μ. The corresponding total phase functions are depicted in Fig. 5(b). Because the simulated R_1 (equal to 2.05 1 Å) is nearly equal to the Ni-0 bond distance of $Ni(OH)_2$, the total- phase (line B) of the Fourier-filtered spectrum approaches the simulated total phase (line A) and the phase-difference fitted line passes through the origin (shown in Fig. 5(c)), as E_0 varies from the first peak of the absorption coefficient to 8 eV above this absorption peak. In other words, due to changing the value of E_0, line B approaches and eventually becomes line C; then lines C and A coincide. The fitted line in Fig. .5(c) yields the Ni-0 bond distance of $Ni(OH)_2$ as (2.0534 ± 0.0017) A. Following similar processes, with the exception of defin-

(a)   (b)   (c)
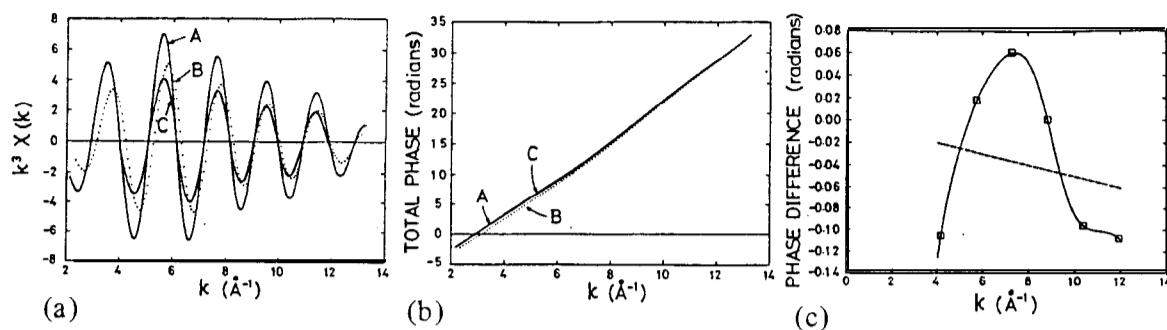
FIG. 5.   (a) The Fourier-filtered $k^3\chi(k)$ spectra of: (1) the simulated data (curve A); (2) the EXAFS
function of $Ni(OH)_2$ extracted by choosing E_0 at the first peak of the absorption coefficient μ
(curve B); (3) the EXAFS function of $Ni(OH)_2$ based on E_0 being 8 eV above the first peak of
the absorption coefficient μ (curve C). (b) Line A is the simulated total phase; lines B and C
illustrate the total phase of the Fourier-filtered spectrum of $Ni(OH)_2$ with different values of E_0
corresponding to (a). (c) The plot of the difference in the total phase functions of the Fourier-
fitted spectra (first shell) of $Ni(OH)_2$, with E_0 chosen at 8eV above the first peak of the absorp-
tion coefficient μ, and of the simulated $Ni(OH)_2$.

ing the simulated $R_1 = 2.057$ Å and the simulated $R_2 = 3.164$ Å, we obtained the phase-
difference fitted line (shown in Fig. 6) which yields the Ni-0 bond distance of $Ni(OH)_2$ as
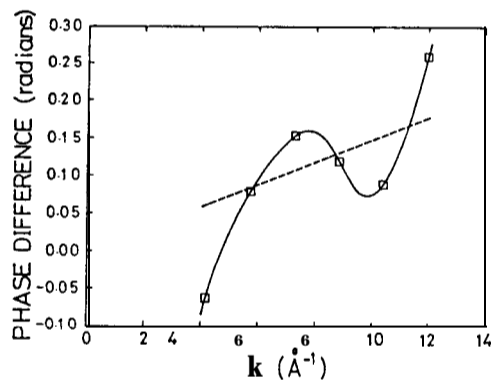(2.0496 ± 0.0018) Å.

FIG. 6.   The total phase difference and the fitted straight line, similar to Fig. 5(c), except that the simulated
$R_1 = 2.057$ Å and $R_2 = 3.164$ Å.

It is notable both that the plot of the magnitude (i.e. the relative heights and the
positions of the first two peaks) of the Fourier-transform of $k^3\chi(k)$ of $Ni(OH)_2$ and the plot
of that of the first two shells of $Ni(OH)_2$ simulated are similar (cf. Fig. 2(b) and Fig. 4(b)),
and that in the case of NiO and the first two shells of NiO simulated the plots of the
magnitudes of the Fourier transform are also similar (cf. Fig. 2(a) and Fig. 7). These results
provide us with the opportunity to identify the surrounding environment of the absorbing
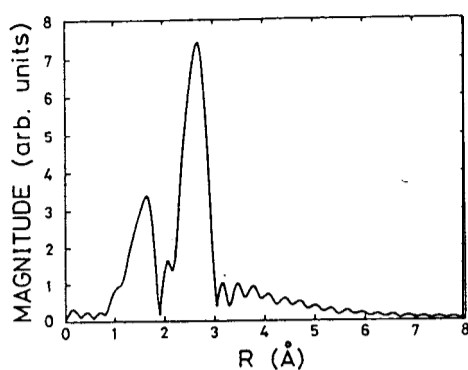atom by comparing the magnitudes of the Fourier transform of the simulated data and the

FIG. 7.   The magnitude of the Fourier transform of the simulated $k^2\chi(k)$ data of NiO, which contains the first two shells ($N_1 = 6$, $N_2 = 12$, $R_1 = 2.08$ Å, $R_2 = 2.94$Å, $\sigma_1^2 = 0.002$, $\sigma_2^2 = 0.002$).

experimental data. It is also notable that, by using the simulated data, we have reconfirmed that the Ni-0 bond distance of $Ni(OH)_2$, which was obtained from the experimental spectrum of the model sample NiO, is approximately equal to (2.05 ~ 2.06) Å. Consequently, by treating the simple case of $Ni(OH)_2$, we have also confirmed that the theoretical data and the experimental data of NiO are reliable.

Assuming that the incorporation of Ni atoms into $YBa_2Cu_3O_{7-y}$ to replace the Cu atoms at either the Cu(1) or the Cu(2) site does not greatly perturb the structure of this material, we can determine that the nearest shells around the Ni atom within $YBa_2Cu_{3-x}Ni_xO_{7-y}$ are formed by oxygen atoms. We obtained the magnitude of the Fourier transform of the $k\chi(k)$ data of $YBa_2Cu_{3-x}Ni_xO_{7-y}$, shown in Fig. 8, by transforming over a k space range 2.28 — 11.78 Å^{-1}. The first two peaks, depicted in Fig. 8, correspond

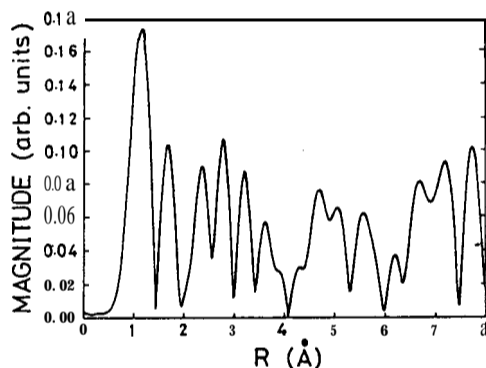FIG. 8.   The magnitude of the Fourier-transform of the $k\chi(k)$ data (K-edge absorption of Ni) of $YBa_2Cu_{3-x}Ni_xO_{7-y}$, obtained by transforming over the k-range 2.28 — **11.78 Å^{-1}** and choosing E_0 at the first peak of the absorption coefficient μ.

to the nearest two shells around the Ni atom within $YBa_2Cu_{3-x}Ni_xO_{7-y}$. These two peaks are too close to each other to resolve the contribution of each peak from an inverse Fourier transform. Therefore, the contribution of the first two peaks, taken together, must be distinguished from that of the other peaks. The Fourier-filtered $\chi(k)$ data, as shown in Fig.

9(a), contains these two unresolved shells. The total phase of the Fourier-filtered $\chi(k)$ spectrum (first two shells) of $YBa_2Cu_{3-x}Ni_xO_{7-y}$ is depicted in Fig. 9(b). According to the beat-node method, the minimum point (beat-node) of the amplitude of the Fourier-filtered $\chi(k)$ data, and the associated kink in the total phase (at $k_b = 7.3$ $Å^{-1}$), shown in Fig. 9(a) and 9(b), indicate that the difference of the bond distances of the nearest two shells $(\Delta R = R_2 - R_1)$ is equal to 0.215 Å. Fig. 9(c) shows the magnitude of the Fourier transform of the Fourier-filtered $k^2\chi(k)$, which we obtained by repeating the Fourier transform.
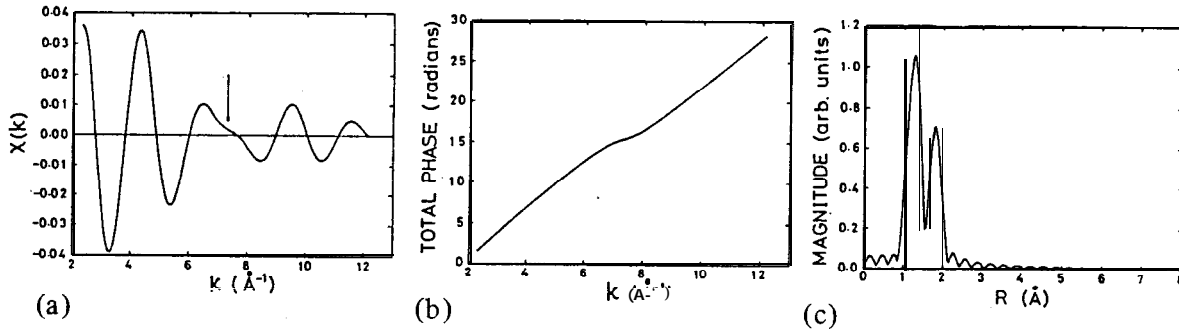

FIG. 9.   (a) The inverse transform (the Fourier-filtered $\chi(k)$ spectrum) from the unresolved 1 st and 2nd shells of $YBa_2Cu_{3-x}Ni_xO_{7-y}$. Here, E_0 is chosen at the half-height point of the absorption edge. The beat at 7.3 $Å^{-1}$ is indicated. (b) The total phase of the Fourier-filtered $\chi(k)$ spectrum depicted in (a). (c) The magnitude of the Fourier transform of the Fourier-filtered $k^2\chi(k)$ spectrum depicted in (a) (over the range 2.65 — 12.00 $Å^{-1}$).

In this case, the approach to obtain more information is to analyze the Fourier-filtered $\chi(k)$ data through the application of the method of fitting. This we accomplished by the use of the appropriate reference compounds for the back-scattering amplitudes and phases. We fitted the Fourier-filtered $\chi(k)$ data of $YBa_2Cu_{3-x}Ni_xO_{7-y}$ by using empirical amplitudes and phases determined from the crystalline NiO for Ni-0 bonds. The $k^{3.4}\chi(k)$ data (shown in Fig. 10(a)) was synthesized with the parameter values $N_1 = 2, N_2 = 2, R_1 = 1.83 \pm 0.01$ Å, $R_2 = 2.04 \pm 0.01$ A, $\sigma_1^2 = 0.002$, $\sigma_2^2 = 0.002$ in order to obtain a shape of the curve of the synthesized $k^{3.4}\chi(k)$ data which is similar to that of the Fourier filtered $\chi(k)$ data of $YBa_2Cu_{3-x}Ni_xO_{7-y}$ (the discrepancy between the k-weighting exponents of the synthesized $k^{3.4}\chi(k)$ data and the Fourier-filtered $\chi(k)$ data of $YBa_2Cu_{3-x}Ni_xO_{7-y}$ is caused by the different ways of processing the raw data). That these fitting results are correct is proved by the consistency of the difference of the bond distances obtained independently based on the beat-node method. The total phase of the synthesized $\chi(k)$ spectrum is depicted in Fig. 10(b), in which the dashed curve refers to the total phase of the Fourier-filtered $\chi(k)$ data of $YBa_2Cu_{3-x}Ni_xO_{7-y}$. This fitting is so nearly perfect that the dashed curve and the solid curve, which refers to the total phase of the synthesized $\chi(k)$ spectrum, coincide almost completely. Furthermore, it is notable that the total phase of the $\chi(k)$ spectrum of the two unresolved shells is not only dependent on R_1 and R_2 but also related to N_1 and N_2 and to the type of atoms involved. By means of other combinations of the values of N_1 and N_2,

except $N_1 = N_2 = 2$, it is impossible to tit the total phase of the Fourier-filtered $\chi(k)$ of $YBa_2Cu_{3-x}Ni_xO_{7-y}$ as well as that shown in Fig. 10(b). Therefore the fact that the fitting is nearly perfect also supports the conclusion that the nearest two shells around the Ni atom in $YBa_2Cu_{3-x}Ni$, O_{7-y} contain atoms of the same type. The plot of the magnitude (i.e. the relative heights and the positions of the first two peaks) of the Fourier transform of the $k^{5.4}\chi(k)$ data, synthesized with the empirical NiO data (shown in Fig. 10(c)), is similar to that of the Fourier transform of the Fourier-filtered $k^2\chi(k)$ spectrum of $YBa_2Cu_{3-x}Ni_xO_{7-y}$

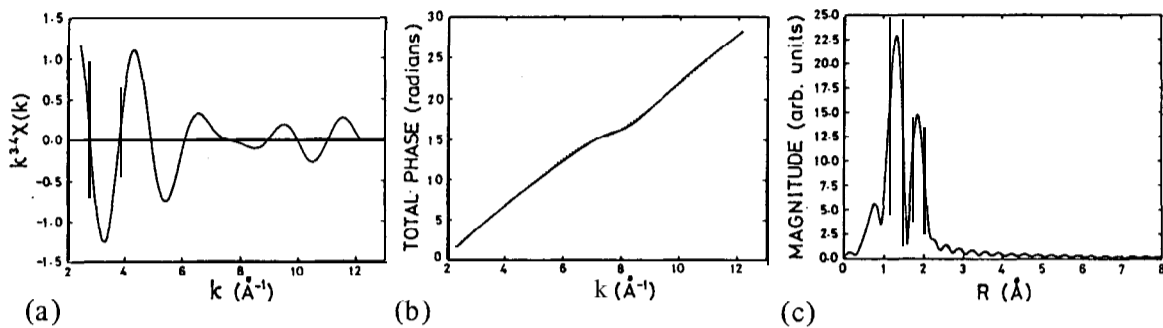(a)   (b)   (c)

FIG. 10.   (a) The $k^{3.4}\chi(k)$ data, which was synthesized with empirical amplitudes and phases obtained from crystalline NiO for Ni-0 bonds. (b) The total phase of the synthesized $\chi(k)$ spectrum (solid curve), and the total phase of the Fourier-filtered $\chi(k)$ spectrum, depicted in Fig. 9(b) (dashed curve). (c) The magnitude of the Fourier transform of the synthesized $k^{5.4}\chi(k)$ spectrum (over the range 2.50 − 11.80 A-'). The small peak at ~ 0.7 Å corresponds to noise.

(cf. Fig. 10(c) and Fig. 9(c)).

By using the theoretical back-scattering amplitudes and phase-shift functions, as we did in the cases of crystalline NiO and $Ni(OH)_2$, we simulated the $\chi(k)$ spectrum of the nearest two shells around the Ni atom within $YBa_2Cu_{3-x}Ni_xO_{7-y}$ with the following structural parameters $N_1 = 2$, $N_2 = 2$, $R_1 = 1.83Å$, $R_2 = 2.038Å$, $\sigma_1^2 = 0.0021$ and $\sigma_2^2 = 0.0021$. Fig. 1 1(a) illustrates the total phase of the simulated $\chi(k)$ spectrum. Although there is a difference 2π in the total phase, due to numerical calculation (and lacking physical meaning), and the task of adjusting the value of E_0 has not been accomplished, the simulated total phase is still qualitatively similar to the total phase obtained from the experimental data of $YBa_2Cu_{3-x}Ni_xO_{7-y}$. By comparing the magnitudes of the Fourier transform of (1) the experimental data and of (2) the simulated data (shown in Fig. 1 1(b)), we reconfirm qualitatively that each of the nearest two shells around the Ni atom contains two oxygen atoms at the distance about $R_1 = 1.83$ A and $R_2 = 2.04$ Å, respectively.

IV. CONCLUSION

The success of our approach is due partly to the fact that the structure of the undoped $YBa_2Cu_3O_{7-y}$ is known and that the possible surrounding environments of the different
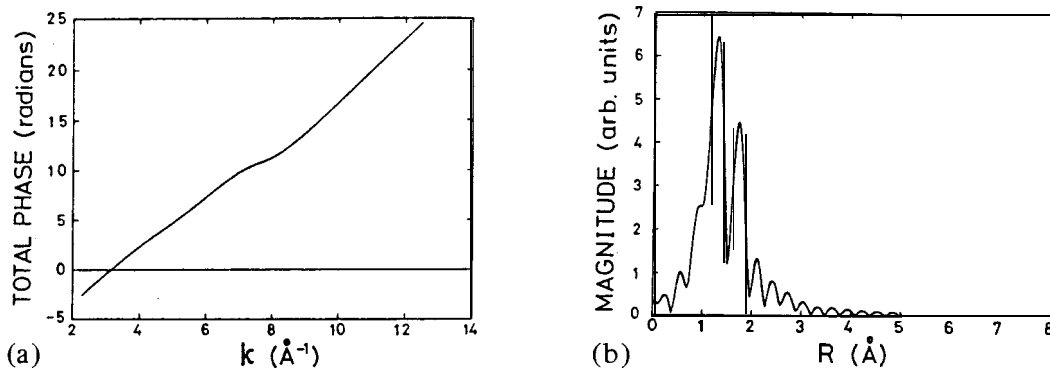
FIG. 11.   (a) The total phase of the simulated $\chi(k)$ spectrum, (b) The magnitude of the Fourier transform of the simulated $k^3\chi(k)$ spectrum (over the range $2.20 - 12.60$ $Å^{-1}$).

sites of the incorporated atom are such that they could be anticipated.

Our results show conclusively that there are two oxygen atoms at a distance R_1 = 1.83 A and another two oxygen atoms at a greater distance R_2 = *2.04* Å around the x-ray-absorbing Ni atom.   This feature strongly suggests that the surrounding environment of the incorporated Ni atom in $YBa_2Cu_{3-x}Ni_xO_{7-y}$ is similar to that of the Cu atom at the Cu(1) site: the two environments vary primarily in that the Ni-0 bond distance is greater than the original Cu-0 bond distance.   (as we might expect, given that the Ni-0 bond distance in nickel oxides is greater than the Cu-O bond distance in copper oxides) In other words, the incorporated Ni atoms preferentially replace a portion of the Cu atoms at the Cu(1) site.

We have demonstrated the power of the EXAFS technique in resolving the local structure of a material as used with the materials of concern in this paper. Although neutron-diffraction measurement is also powerful in determining the location of the impurities in materials, the advantages of EXAFS are that it is less difficult in terms of sample requirement and that the process can be implemented even with ordinary rotating anodes in the x-ray source.

ACKNOWLEDGMENTS

REFERENCES

1.   R. J. Cava, B. Batlogg, C. H. Chen, E. A. Rietman, S. M. Zahurak and D. Werder, Phys. Rev. B36, 5719 (1987).

2. T. Siegrist, S. Sunshine, D. W. Murphy, R. J. Cava and S. M. Zahurak, Phys. Rev. B3.5, 7137 (1987).

3. J. D. Jorgensen, B. W. Veal, W. K. Kwok, G. W. Crabtree, A. Umezawa, L. J. Nowicki and A. P. Paulikas, Phys. Rev. B36, 573 1 (1987).

4. J. D. Jorgensen, M. A. Beno, D. G. Hinks, L. Soderholm, K. J. Volin, R. L. Hitterman, J. D. Grace and Ivan K. Schuller, Phys. Rev. B36, 3608 (1987).

5. Gang Xiao, M. Z. Cieplak, A. Gavrin, F. H. Streitz, A. Bakhshai and C. L. Chien, Phys. Rev. Lett. 60, 1446 (1988).

6. T. Siegrist, L. F. Schneemeyer, J. V. Waszczak, N. P. Singh, R. L. Opila, B. Batlogg, L. W. Rupp and D. W. Murphy, Phys. Rev. B36, 8365 (1987).

7. D. C. Koningsberger, R. Prins, Principles, Applications, Techniques of EXAFS, SEXAFS and XANES, John Wiley & Sons, Inc., New York, (1988).

8. J. J. Boland, F. G. Halaks and J. D. Baldeschweiler, Phys. Rev. B28, 2921 (1983).

9. A. G. Mckale, B. W. Veal, A. P. Daulikas, S.-K. Chan and G. S. Knapp, J. Am. Chem. Soc., 110, 3763 (1988).

10. A. G. Mckale, G. S. Knapp, S.-K. Chan, Phys. Rev. B33, 841 (1986).

11. Ref 7, PP 603.

12. Boon-Keng Teo, P. A. Lee, J. Am. Chem. Soc., 101, 2815 (1979).